Johnson Robert T (Orcid ID: 0000-0003-3618-238X)

Jørgensen Helle F (Orcid ID: 0000-0002-7909-2977)

Piezo1-mediated regulation of smooth muscle cell volume in response to enhanced extracellular matrix rigidity

Robert T. Johnson[1*], Reesha Solanki[1*], Finn Wostear[1*], Sultan Ahmed[1], James C.K. Taylor[2], Jasmine Rees[1], Geraad Abel[1], James McColl[3], Helle F. Jørgensen[2], Chris J. Morris[4], Stefan Bidula[1] and Derek T. Warren[1+]

[1] School of Pharmacy, University of East Anglia, Norwich Research Park, Norwich, NR4 7TJ, UK.

[2] Section of Cardiorespiratory Medicine, University of Cambridge, VPD Heart and Lung Research Institute, Papworth Road, Cambridge Biomedical Campus, Cambridge, CB2 0BB, UK

[3] Henry Wellcome Laboratory for Cell Imaging, University of East Anglia, Norwich Research Park, Norfolk. NR4 7TJ, UK

[4] School of Pharmacy, University College London, London, United Kingdom.

* Contributed equally to this study

[+] Corresponding Author: Dr. Derek Warren (derek.warren@uea.ac.uk)
School of Pharmacy, University of East Anglia, Norwich Research Park, Norwich, Norfolk, UK, NR4 7TJ

ORCiD IDs: RTJ (https://orcid.org/0000-0003-3618-238X)

RS (https://orcid.org/0009-0002-4652-1832)

FW (https://orcid.org/0009-0003-0703-8917)

HJF (https://orcid.org/0000-0002-7909-2977)

This article has been accepted for publication and undergone full peer review but has not been through the copyediting, typesetting, pagination and proofreading process which may lead to differences between this version and the Version of Record. Please cite this article as doi: 10.1111/bph.16294

CJM (https://orcid.org/0000-0002-7703-4474)

SB (https://orcid.org/0000-0002-3790-7138)

DTW (https://orcid.org/0000-0003-0346-7450)

Running Title: Piezo1 mediated control of smooth muscle cell volume

Word Count: 7,019

Abstract

Background and Purpose: Decreased aortic compliance is a precursor to numerous cardiovascular diseases. Compliance is regulated by the rigidity of the aortic wall and the vascular smooth muscle cells (VSMCs). Extracellular matrix stiffening, observed during ageing, reduces compliance. In response to increased rigidity, VSMCs generate enhanced contractile forces that result in VSMC stiffening and a further reduction in compliance. Mechanisms driving VSMC response to matrix rigidity remain poorly defined.

Experimental Approach: Human aortic-VSMCs were seeded onto polyacrylamide hydrogels whose rigidity mimicked either healthy (12 kPa) or aged/diseased (72 kPa) aortae. VSMCs were treated with pharmacological agents prior to agonist stimulation to identify regulators of VSMC volume regulation.

Key Results: On pliable matrices, VSMCs contracted and decreased in cell area. Meanwhile, on rigid matrices VSMCs displayed a hypertrophic-like response, increasing in area and volume. Piezo1 activation stimulated increased VSMC volume by promoting calcium ion influx and subsequent activation of PKC and aquaporin-1. Pharmacological blockade of this pathway prevented the enhanced VSMC volume response on rigid matrices whilst maintaining contractility on pliable matrices. Importantly, both piezo1 and aquaporin-1 gene expression were upregulated during VSMC phenotypic modulation in atherosclerosis and after carotid ligation.

Conclusions and Implications: In response to extracellular matrix rigidity, VSMC volume is increased by a piezo1/PKC/aquaporin-1 mediated pathway. Pharmacological targeting of this pathway specifically blocks the matrix rigidity enhanced VSMC volume response, leaving VSMC contractility on healthy mimicking matrices intact. Importantly, upregulation of both piezo1 and aquaporin-1 gene expression is observed in disease relevant VSMC phenotypes.

Bullet point summary:

- Vascular smooth muscle cells (VSMC) possess increased volume of rigid hydrogels
- Actomyosin activity is required for this increased volume response
- Piezo1 activity permits calcium ion influx into VSMCs on rigid hydrogels
- Pharmacological inhibition of PKC or aquaporin-1 block the enhanced VSMC response on rigid hydrogels
- PKC inhibition prevents translocation of aquaporin-1 to the VSMC cell membrane
- Piezo1 and aquaporin-1 gene expression is increased in disease relevant VSMC phenotypes in atherosclerosis and after carotid ligation

1. Introduction

Aortic compliance describes the ability of the aorta to change shape in response to changes in blood pressure. Maintaining aortic compliance is essential for cardiovascular (CV) health and decreased aortic compliance is a major risk factor associated with a variety of age-related CV diseases (Glasser et al., 1997; Mitchell et al., 2010; Lacolley et al., 2020). Clinical measurements of aortic compliance, using pulse wave velocity, identify that reduced compliance is associated with increased CV mortality (Safar et al., 2002; Zhong et al., 2018; Sequí-Domínguez et al., 2020). The rigidity of the aortic wall is a major contributor to aortic compliance. In the healthy aortic wall, rigidity and compliance are determined by the balance between extracellular elastic fibres, including elastin, which provides pliability, and non-elastic extracellular matrix (ECM) components, including collagen-I, that provides tensile strength to the aortic wall (Tsamis et al., 2013). However, during ageing and CV disease, elastic-fibres degrade, and collagen-I accumulates. These ECM changes increase the rigidity of the aortic wall and decrease aortic compliance (Ahmed and Warren, 2018).

Vascular tone is regulated by the contraction of vascular smooth muscle cells (VSMCs), the predominant cell type within the aortic wall (Leloup et al., 2019). These mechanosensitive cells generate actomyosin-derived forces, with force production increasing as ECM rigidity increases (Petit et al., 2019; Sanyour et al., 2019; Johnson et al., 2021). Enhanced actomyosin force generation increases VSMC stiffness and in turn contributes to increased aortic wall rigidity and reduced aortic compliance observed in ageing and CV disease (Qiu et al., 2010; Sehgel et al., 2015b; Lacolley et al., 2017). In healthy aortae, wall rigidity and compliance are a balance between ECM rigidity and VSMC stiffness (Johnson et al., 2021). However, this balance is disrupted in ageing and CV disease, resulting in VSMC dysfunction (Sazonova et al., 2011; Lacolley et al., 2017). For example, in hypertension, aortic stiffness increases as a result of enhanced ECM rigidity and VSMC hypertrophy, a process through which cell mass increases without a corresponding increase in cell number (Owens and Schwartz, 1983; Rizzoni et al., 2000; Zhang et al., 2005; Schiffrin, 2012; Sehgel et al., 2013). VSMC hypertrophy increases aortic wall thickness and rigidity, resulting in reducing aortic compliance (Zieman et al., 2005; Hayashi and Naiki, 2009; Sehgel et al., 2015a). Both increased protein content and increased volume are key components of VSMC hypertrophy, yet mechanisms regulating VSMC volume remain poorly defined.

Other cell types contain mechanisms to reduce or increase cell volume in response to swelling or shrinking, respectively (McManus et al., 1995; Hoffmann et al., 2009). These pathways involve ion transporters that result in the movement of ions across the plasma membrane to create solute gradients. For example, cell swelling activates volume regulated anion channels (VRACs) that result in the efflux of chloride ions, whereas cell shrinking activates $Na^+.K^+.2Cl^-$ (NKCC), resulting in chloride ion influx (Eggermont et al., 2001). Aquaporins are essential components of these processes and regulate the movement of water across membranes (Mola et al., 2016). This process is passive and driven by solute gradients across the plasma membrane. Importantly, water follows the chloride ions due to osmosis. Therefore, chloride ion and water influx promote cell swelling, whereas efflux promotes cell shrinking (Morishita et al., 2019). In addition to chloride ion concentration

changes, post-translational modification status of the aquaporins also regulate their activity. For example, aquaporin-1 phosphorylation by PKC triggers aquaporin-1 translocation to the plasma membrane, activating aquaporin-1 mediated water influx and increasing cell volume (Conner et al., 2010). VSMCs express aquaporin-1, however, the importance of this water channel in VSMC volume regulation and VSMC dysfunction remains unknown (Shanahan et al., 1999).

In response to matrix rigidity, ECM adhesions activate the Rho/ROCK signalling pathway, resulting in actin polymerisation and myosin light chain phosphorylation, that in turn enhance actomyosin activity (Ahmed and Warren, 2018). In other cell types, actomyosin activity and actin cytoskeleton reorganisation in response to ECM rigidity have been shown to activate stretch activated ion channels (SACs) (Kobayashi and Sokabe, 2010; Nourse and Pathak, 2017). SAC activation enables mechanical stimuli to be converted into biochemical responses through mediating the diffusion of ions, including calcium ions (Ca^{2+}), across the cell membrane (Kobayashi and Sokabe, 2010). Whether VSMCs possess a similar response to ECM rigidity remains unknown, however, VSMCs possess numerous stretch activated ion channels including piezo1 and members of the TRP (transient receptor potential) family (Lowis et al., 2023). In normal physiology, these channels are activated transiently by blood flow derived stretching of the aortic wall (Liu and Lin, 2022). This stimulates VSMC contraction as a result of Ca^{2+} influx. These SACs are also reported to contribute to VSMC dysfunction, with piezo1 implicated in atherosclerosis and abdominal aortic aneurysm induced vascular remodelling (Qian et al., 2022; Yin et al., 2022). Whether SACs, including piezo1, are involved in VSMC volume regulation and the mechanisms by which they drive VSMC dysfunction remain unknown. Investigating the cellular response to matrix rigidity requires us to move away from the use of tissue culture plastic and glass, materials whose stiffness is around a thousand times greater than that of a healthy aorta (Minaisah et al., 2016). The rigidity of the aortic wall, known as its Young's modulus (measured in kilopascals (kPa)), has been experimentally determined using atomic force microscopy (Hayenga et al., 2011; Tracqui et al., 2011). In this study, we utilised polyacrylamide hydrogels, substrates fabricated to the same rigidity as a healthy or diseased aorta (Hayenga et al., 2011; Tracqui et al., 2011; Minaisah et al., 2016; Rezvani-Sharif et al., 2019). We identify that enhanced ECM rigidity promotes increased VSMC volume following contractile agonist stimulation. This increased volume response is driven by a piezo1/PKC/aquaporin-1 mediated pathway. Inhibition of the piezo1/PKC/aquaporin-1 pathway prevented ECM rigidity induced VSMC volume response whilst leaving VSMC contractility on healthy mimicking substrates unimpeded. Finally, both piezo1 and aquaporin-1 expression is enhanced during VSMC phenotypic modulation in atherosclerosis and after carotid ligation.

2. Methods

2.1 Polyacrylamide Hydrogel Preparation

Hydrogels were prepared as described previously (Minaisah et al., 2016). Glass coverslips were activated by treating with (3-Aminopropyl)triethoxysilane for 2 minutes, washed 3x in dH_2O, then fixed in 0.5% glutaraldehyde for 40 minutes. After fixation, coverslips were washed and left to air dry overnight. Polyacrylamide hydrogel buffer was comprised as follows: 12 kPa – 7.5% acrylamide, 0.15% bis-acrylamide in dH_2O; 72 kPa – 10% acrylamide, 0.5% bis-acrylamide in dH_2O. To prepare hydrogels for fabrication, the appropriate volume of buffer was supplemented with 10% APS (1:100) and TEMED (1:1,000) then placed on a standard microscopy slide and covered by an activated coverslip (13 mm coverslips required 30 µl of supplemented buffer; 33 mm coverslips used 50 µl). Once set, the hydrogels were washed 3x in dH_2O to remove any unpolymerized acrylamide, crosslinked with sulfo-SANPAH (1:3,000) under UV illumination (365 nm) for 5 minutes, then functionalised with collagen I (0.1 mg/ml) for 10 minutes at room temperature. Hydrogel stiffnesses have previously been confirmed using a JPK Nanowizrd-3 atomic force microscope (Porter et al., 2020). These hydrogels are used extensively in cell biological research with no loss of viability when compared to tissue culture plastic or glass (Minaisah et al., 2016; Porter et al., 2020).

2.2 Vascular Smooth Muscle Cell Culture

Human adult aortic VSMCs were purchased from Cell Applications Inc. (354-05a). Standard VSMC culture (passages 3-9) was performed as previously described (Ragnauth et al., 2010; Warren et al., 2015). VSMCs were seeded onto polyacrylamide hydrogels in basal media (Cell Applications Inc Cat# 310-500), 18 hours prior to the beginning of the experiment. Briefly, VSMCs were pre-treated with pharmacological agents for 30 minutes, prior to co-treatment with a contractile agonist for an additional 30 minutes. Experimental specific concentrations are provided in the corresponding figure legends. Please see **Supplementary Table S1** for details of compounds used in this study. VSMCs were pretreated with the concentration range of vehicle control (DMSO) alone that was used for the drug screening component of this study. The DMSO alone pretreatment has no effect on angiotensin II stimulated VSMC area on 12 and 72 kPa hydrogels (**Supplementary Figure S1**). Working concentrations of the compounds used in this study had no effect on the area of quiescent VSMCs (**Supplementary Figure S2**) For experiments where working concentrations of the compounds used in this study, DMSO vehicle control pre-treatments were also performed. For experiments performed in basal and growth media, VSMCs were seeded onto 12 and 72 kPa hydrogels and incubated in the relevant media for 24 hours prior to drug treatments. For pharmacological agents were added at the working concentration of the pharmacological agent or DMSO vehicle control and cells were incubated for 18 hours.

2.3 Immunofluorescence and VSMC Area/Volume Analysis

Cells were fixed in 4% paraformaldehyde for 10 minutes, permeabilised with 0.5% NP40 for 5 minutes, then blocked with 3% BSA/PBS for 1 hour. Primary staining against lamin A/C (1:200) (Sigma-Aldrich Cat# SAB4200236, RRID:AB_10743057) was performed overnight at 4 °C in 3% BSA/PBS. Secondary staining was performed using the appropriate Alexa Fluor™

488 antibody (1:400) (Thermo Fisher Scientific Cat# A-11001, RRID:AB_2534069) in the dark for 2 hours. F-actin was visualised using Rhodamine Phalloidin (1:400) (Thermo Fisher Scientific Cat# R145). Images were captured at 20x magnification using a Zeiss LSM980-Airyscan confocal microscope. Cell area and volume was measured using FIJI, open-source software (Schindelin et al., 2012; Ahmed et al., 2022) Briefly, channels were separated using the split channel function. The F-actin image was thresholded on the brightest slice using the Otsu method to remove gaps. The cell edge was drawn around using the region of interest (ROI) function. Cell area was measured on the image of the nuclei and recorded by selecting the ROI on the image. In the set measurements menu, area and limited to threshold options were selected before the total volume of thresholded objects was calculated by running the ImageJ macro code freely available from Visikol at https://visikol.com/blog/2018/11/29/blog-post-loading-and-measurement-of-volumes-in-3d-confocal-image-stacks-with-imagej/

2.4 Fluo-4 Calcium imaging

Cells seeded on 12 and 72kPa hydrogels and incubated in basal medium for 48 hours. Cells were loaded with 3 µM Fluo-4 AM (ThermoFisher Scientific cat #F14201) diluted in basal media for 30 minutes. GsMTx-4, Yoda1 and A23187 were used at working concentrations listed in Supplementary Table 1. For GsMTx-4 experiments, cells were co-treated with vehicle control or GsMTx-4 during the Fluo-4 loading step. Cells were washed in PBS and incubated in basal media prior to imaging. Cells were placed onto a Zeiss Axiovert 200M inverted microscope stage and images were captured every 500 ms. Cells were imaged for 5 minutes prior to angiotensin II (10 µM) stimulation. For Yoda1 treatments, angiotensin II and Yoda1 were added at the same time. Cells were subsequently imaged for a further 20 minutes after addition of angiotensin II. Finally, the ionophore A23187 was added for a further 5 minutes to confirm the calcium imaging had worked. Images were analysed in ImageJ by selecting a ROI and extracting the fluorescence intensities for each time point using the plot Z-axis profile option. Background was subtracted and the ΔF and $\Delta F/F_0$ values were calculated and analysed using GraphPad prism.

2.5 Cell Viability Assay

Cell viability was determined using a RealTime-Glo™ MT Cell Viability Assay (Promega), as per manufacturer's instructions. Briefly, 5,000 cells per well seeded in a 96-well plate and exposed to a range of drug concentrations for 1 hour. Luminescence was subsequently measured using a Wallac EnVision 2103 Multilabel Reader (PerkinElmer).

2.6 siRNA Knockdown

VSMC siRNA transfection was performed using HiPerFect (Qiagen) as per manufacturer's instructions, the day before cells were seeded onto hydrogels. VSMCs were transfected with either scrambled siRNA control or piezo1 targeting siRNA (listed below) oligos. The next afternoon, cells were seeded onto hydrogels as above, serum was withdrawn overnight to induce quiescence and the next morning VSMCs were stimulated with Angiotensin II (10 µM) for 30 minutes prior to fixation and downstream immunofluorescent analysis.

siRNA #5 – CCGCGTCTTCCTTAGCCATTA

siRNA #7 – CGGCCGCCTCGTGGTCTACAA

2.7 Western Blotting

Western blotting was performed as previously described (Ragnauth et al., 2010). When looking for piezo1 expression specifically, lysates were run on a TruPAGE precast 4-20% gradient gel (Sigma-Aldrich) at 120 V for 2 hours. Protein was transferred onto PVDF membrane at 30 V for 3 hours prior to the membrane being blocked in 5% milk/TBST. The following antibodies were used: anti-piezo1 (1:500) (Novus Cat# NBP1-78537, RRID:AB_11003149), anti-GAPDH (1:4000) (Cell Signalling Technology Cat# 2118, RRID:AB_561053) and anti-Rabbit-HRP (1:2000) (Sigma-Aldrich Cat# GENA934, RRID:AB_2722659).

2.8 Single cell-RNA sequencing data analysis

scRNA-seq profiles of lineage-traced, FACS-isolated VSMCs from the aortic arch and carotid arteries of Myh11-CreERt2; Rosa26-Confetti+; Apoe-/- animals analysed after 14-18 weeks high fat diet (Dobnikar et al., 2018) or from injured left carotids of Myh11-CreERt2; Rosa26-EYFP+ animals analysed 5 or 7 days after carotid ligation surgery (Worssam et al., 2023) were retrieved from the gene expression omnibus (accession GSE117963, GSE235805). The data was analysed as described (Worssam et al., 2023) and sctransform-normalised gene expression levels and cell cluster identities mapped onto uniform manifold approximation and projections (UMAPs). For the day 5 injury dataset, a heatmap showing genes clustered according to their expression along cells ordered by their progression along a proliferation-associated pseudotime (Worssam et al., 2023) was generated using pheatmap (1.0.12).

2.9 Statistical Analysis

The data and statistical analysis in this study complies with the recommendations on experimental design and analysis in pharmacology (Curtis et al., 2018). Experiments were performed by one researcher, with a second researcher then performing the microscopy and downstream analysis. Statistical analysis was performed using GraphPad Prism 9.5. Results are presented as mean ± SEM, with mean data points for each individual experiment shown in black dots. The number of independent repeats performed, and total number of cells analysed per experiment are detailed in the corresponding figure legend. Normality testing was performed, using the Shapiro-Wilk normality test and all data display a normal distribution. Unpaired Student's t-tests were used for the comparison of two conditions. To compare concentration responses at a single hydrogel stiffness, one-way ANOVA was performed, with either a Tukey's or Sidak's multiple comparison post-hoc test being performed as appropriate. Concentration-response curves are presented as mean ± SEM plotted on a logarithmic scale. Log(agonist) vs response curves were generated using non-linear regression. Comparisons between concentration ranges on different hydrogel stiffness were performed using a two-way ANOVA followed by Sidak's multiple comparison test. To compare multiple groups in the volume analysis, two-way ANOVA was performed followed

by a Tukey's multiple comparison test. Differences between conditions were considered statistically significant when $P < 0.05$.

2.10 Nomenclature of Targets and Ligands

Key protein targets and ligands in this article are hyperlinked to corresponding entries in http://www.guidetopharmacology.org, and are permanently archived in the Concise Guide to PHARMACOLOGY 2021/22 (Alexander et al., 2021).

3. Results

3.1 Matrix rigidity alters isolated smooth muscle cell response to contractile agonist stimulation.

We set out to determine how enhanced matrix rigidity, akin to that of an aged/diseased aortic wall, would affect VSMC response to contractile agonists. Quiescent VSMCs grown on pliable (12 kPa) or rigid (72 kPa) hydrogels were stimulated with increasing concentrations of the contractile agonist angiotensin II. Changes in VSMC area were used as a measure of contractile response (Ahmed et al., 2022). As previously observed, VSMCs on pliable hydrogels contracted, indicated by a decrease in cell area as angiotensin II concentration increased (**Figure 1A, B & D**) (Ahmed et al., 2022). In contrast, VSMCs seeded on rigid hydrogels were initially smaller than those on pliable hydrogels, yet when exposed to increasing concentrations of angiotensin II, cell area increased (**Figure 1A, C & D**). Stimulation of VSMCs with increasing concentrations of an alternative contractile agonist, carbachol, again resulted in a differential response whereby VSMC area was reduced on pliable hydrogels but increased on rigid hydrogels (**Figure 1E-H**). Subsequent experiments were performed by stimulating VSMCs with 10 μM of either angiotensin II or carbachol, a concentration which induced maximal area changes on both rigidities of hydrogel.

To confirm that the above changes were specific for receptor activation, we utilised the receptor antagonists irbesartan and atropine. Irbesartan antagonises the angiotensin II type 1 receptor, AT1R, whilst atropine antagonises acetylcholine receptors thereby blocking the effects of carbachol. Quiescent VSMCs grown on pliable or rigid hydrogels were stimulated with either angiotensin II or carbachol in the presence of an increasing concentration of their respective antagonist. On pliable hydrogels, increasing concentrations of irbesartan or atropine prevented VSMCs from undergoing a contractile response (**Supplementary Figures S3 and S4**). Likewise, treatment with irbesartan or atropine prevented contractile agonist induced enlargement of VSMCs on rigid hydrogels (**Supplementary Figures S3 and S4**).

3.2 Isolated smooth muscle cells display increased volume on rigid substrates following contractile agonist stimulation.

The above data demonstrates that VSMC response to contractile agonist stimulation is regulated by matrix rigidity. We next sought to determine whether VSMC volume, as well as area was enlarged following contractile agonist stimulation on rigid substrates. To test this, quiescent VSMCs were seeded on pliable and rigid hydrogels and stimulated with angiotensin

II. Confocal microscopy was used to measure VSMC volume. As previously observed (Ahmed et al., 2022), VSMCs on pliable hydrogels underwent a contractile response following angiotensin II stimulation, decreasing in cell area but displaying no change in volume (**Figure 2A-C**). In contrast, angiotensin II stimulation of VSMCs on rigid hydrogels resulted in both cell area and volume enlargement, cell height remained unaltered (**Figure 2A-C**). We next tested whether the matrix rigidity induced increase in VSMC volume persisted in the longer term, by performing confocal microscopy of VSMCs incubated in basal or growth media on pliable and rigid hydrogels. Analysis revealed that there were no significant differences in area or volume of VSMCs incubated in basal or growth media for 24 hours on pliable hydrogels (**Figure 2E-G**). In contrast, VSMCs incubated in growth media on rigid hydrogels possess increased area and volume compared to their basal media incubated counterparts (**Figure 2E-G**). Importantly, VSMCs incubated in growth media for 24 hours on rigid hydrogels possessed increased area and volume, compared to their growth media treated counterparts on pliable hydrogels (**Figure 2E-G**). No changes in cell height were observed in any condition (**Figure 2D and H**).
Next, we predicted that the matrix rigidity induced volume response was driven by actomyosin activity and intracellular tension. To test this, quiescent VSMCs seeded on pliable and rigid hydrogels were pretreated with the non-muscle myosin II inhibitor blebbistatin, prior to angiotensin II stimulation. Analysis revealed that blebbistatin treated VSMCs on pliable hydrogels prevented the decrease in VSMC area upon angiotensin II stimulation and were larger than their vehicle treated counterparts (**Figure 3A and B**). Volume also tended to be increased in blebbistatin treated VSMCs on pliable hydrogels, compared to their vehicle treated counterparts, but this difference was not significant (**Figure 3A and C**). In contrast, blebbistatin treated VSMCs on rigid hydrogels possessed decreased area and volume, compared to their vehicle treated counterparts (**Figure 3A-C**). VSMC height remained similar in all conditions (**Figure 3D**).

3.3 Piezo1 activity contributes to the increased VSMC volume response on rigid hydrogels

The above data shows that in response to actomyosin activity, VSMCs undergo contraction on pliable hydrogels, but display an increased volume response on rigid hydrogels. Angiotensin II mediated activation of the AT1R receptor drives Ca^{2+} release from the sarcoplasmic reticulum, increasing cytosolic Ca^{2+} levels (Woodrum and Brophy, 2001). Therefore, we next investigated whether ECM rigidity promoted differences in intracellular Ca^{2+} handling. Quiescent VSMCs were pre-treated with an increasing concentration of the ryanodine receptor antagonist dantrolene, prior to angiotensin II stimulation. On pliable hydrogels, increasing concentrations of dantrolene prevented VSMCs from undergoing a contractile response and displayed increased cell area (**Supplementary Figure S5A, B and D**). Likewise, dantrolene pretreatment prevented the angiotensin II induced enlargement of VSMCs on rigid hydrogels (**Supplementary Figure S5A, C and D**). Dantrolene treatment had no effect on VSMC viability (**Supplementary Figure S5E**). This suggested that sarcoplasmic Ca^{2+} release was a common component of both the contractile and hypertrophic response. We next confirmed the impact of dantrolene treatment on VSMC volume by confocal microscopy. Dantrolene pretreatment had no effect on angiotensin II stimulated VSMC volume on pliable hydrogels compared to their vehicle control treated counterparts (**Supplementary Figure S6**). In contrast, dantrolene pretreatment reduced the angiotensin II

stimulated VSMC volume on rigid hydrogels compared to their vehicle control treated counterparts (**Supplementary Figure S6**)

ECM rigidity is known to promote the activation of SACs, enabling the influx of extracellular Ca^{2+} in a variety of cell types (Emig et al., 2021; Li et al., 2022; Lopez-Cavestany et al., 2023; Wu et al., 2023). To test whether this was also true in VSMCs, we next utilised the SAC blocker, GsMTx-4. Quiescent VSMCs were pre-treated with an increasing concentration of GsMTx-4 prior to angiotensin II treatment on pliable and rigid hydrogels. Analysis revealed that GsMTx-4 pre-treatment had no effect on VSMC area on pliable hydrogels (**Supplementary Figure S7A, B and D**). In contrast, GsMTx-4 pre-treatment blocked the increase in VSMC area on rigid hydrogels in a concentration dependent manner (**Supplementary Figure S7A, C and D**). GsMTx-4 pre-treatment had no effect on the viability of VSMCs (**Supplementary Figure S7E**). To confirm that changes in VSMC area correlated with changes in volume, we next performed confocal microscopy on GsMTx-4 pre-treated VSMCs. SAC blockade had no effect on angiotensin II treated VSMC area or volume on pliable hydrogels, compared to the vehicle control treated counterparts (**Figure 4A-C**). However, on rigid hydrogels, GsMTx-4 pre-treatment blocked the angiotensin II induced increases in VSMC area and volume, compared to their vehicle control treated counterparts (**Figure 4A-C**). No changes in VSMC height were observed with any treatment (**Figure 4D**).

To observe whether SAC blockade could reduce VSMC volume in the longer term, VSMCs incubated in growth media on pliable and rigid hydrogels were incubated with GsMTx-4 for 18 hours. Analysis confirmed that GsMTx-4 treatment did not alter VSMC area or volume of VSMCs on pliable hydrogels, compared to their vehicle control treated counterparts (**Figure 4E-G**). In contrast, GsMTx-4 treated VSMCs on rigid hydrogels possessed reduced area and volume, compared to their vehicle treated counterparts (**Figure 4-G**). No changes in VSMC height were observed in any condition (**Figure 4H**).

The above data shows that VSMC hypertrophy on rigid substrates is mediated by SAC activation. Piezo1 is a SAC known to be involved in atherosclerosis and abdominal aortic aneurysm-mediated VSMC dysfunction (Qian et al., 2022; Yin et al., 2022). Whether piezo1 is involved in VSMC volume regulation remains unknown. We therefore investigated its potential role in regulating VSMC response to ECM rigidity by utilising an siRNA mediated knockdown approach. Western blotting confirmed that two independent siRNAs efficiently depleted piezo1 in VSMCs (**Figure 5A and B**). Analysis revealed that piezo1 depletion had no effect on angiotensin II induced VSMC contractility on pliable hydrogels, with no change in VSMC area or volume detected. (**Figure 5C-E**). In contrast, piezo1 depletion blocked the angiotensin II mediated increase in VSMC area and volume on rigid hydrogels (**Figure 5C-E**). No changes in VSMC height were observed in any condition (**Figure 5F**). To confirm that piezo1 depletion reduced VSMC in the longer term, siRNA treated VSMCs were incubated for 24 hours in growth media on pliable and rigid hydrogels. Analysis confirmed that piezo1 depletion had no effect on VSMC area or volume on pliable hydrogels, compared to control depleted VSMCs (**Supplementary Figure S8A-C**). In contrast, piezo1 depleted VSMCs displayed reduced area and volume on rigid hydrogels, compared to their control depleted

counterparts (**Supplementary Figure S8A-C**). No changes in VSMC height were observed in any condition (**Supplementary Figure S8D**).

3.4 Piezo1-mediated Ca^{2+} influx promotes the increased VSMC volume response on rigid hydrogels

The above data implicates piezo1 in the matrix rigidity induced volume response of VSMCs. We next speculated that enhanced piezo1 activity would increase intracellular Ca^{2+} levels and drive increased VSMC volume. To test this, quiescent VSMCs on rigid and pliable hydrogels were loaded with the Ca^{2+} indicator Fluo-4 prior to angiotensin II treatment. Fluorescence video time lapse microscopy was used to measure changes in Fluo-4 fluorescence. Analysis revealed that on pliable hydrogels, angiotensin II stimulation resulted in a rapid increase in intracellular Ca^{2+} levels that rapidly declined back to baseline (**Figure 6 A**). In contrast, angiotensin II stimulation of VSMCs on rigid hydrogels resulted in a rapid increase in intracellular Ca^{2+}, but the peak was smaller and broader than those displayed by VSMCs on pliable hydrogels (**Figure 6A, B and Supplementary Figure S9**). In addition, VSMCs on rigid hydrogels demonstrated a sustained increase in intracellular Ca^{2+} levels and demonstrated multiple smaller peaks that were not present in VSMCs on pliable hydrogels (**Figure 6A, B and Supplementary Figure S9**). GsMTx-4 pretreatment had no effect on the peak values but reduced the sustained Ca^{2+} levels in VSMCs on rigid hydrogels (**Supplementary Figure S10**). To test whether piezo1 activity triggered increased intracellular Ca^{2+} levels, we utilised the piezo1 specific allosteric activator Yoda1. Analysis revealed that Yoda1 treatment did not alter the peak Ca^{2+} levels in angiotensin II treated VSMCs on pliable hydrogels, but it increased the peak Ca^{2+} level of angiotensin II stimulated VSMCs on rigid hydrogels (**Figure 6A-E**). Yoda1 treatment also resulted in a sustained increase in intracellular Ca^{2+} levels in angiotensin II treated VSMCs on both pliable and rigid hydrogels (**Figures 6A-D and F**). Next, we speculated that Yoda1 treatment would increase the volume of angiotensin II stimulated VSMCs on pliable hydrogels. To test this, quiescent VSMCs were stimulated with angiotensin II in the presence or absence of Yoda1. Confocal microscopy analysis revealed that Yoda1 treated VSMCs had increased volume on pliable hydrogels, compared to their vehicle control treated counterparts (**Figure 6G-J**). Yoda1 treatment had no effect on VSMC volume in angiotensin II stimulated VSMCs on rigid hydrogels (**Supplementary Figure S11**).

3.5 PKC and aquaporin-1 activity stimulate the enhanced VSMC volume response on rigid hydrogels

The above data shows that piezo1-mediated Ca^{2+} influx initiates increased VSMC volume on rigid hydrogels. We next sought to delineate the downstream processes that triggered the increase in VSMC volume. We predicted that aquaporin-1 would have a role in this matrix rigidity induced response. To test this, quiescent VSMCs on rigid hydrogels were pretreated with a concentration response of the aquaporin-1 blocker TCAQP1, prior to angiotensin II stimulation. Analysis revealed that VSMCs displayed reduced area as TCAQP1 concentration increased (**Supplementary Figure S12**). Western blot confirmed the presence of aquaporin-1 in VSMCs and suggested that both piezo1 and aquaporin-1 levels were similar on pliable and rigid hydrogels, although piezo1 levels trended towards being reduced on rigid hydrogels (**Supplementary Figure S12C-E**). Furthermore, confocal microscopy confirmed that

TCAQP1 treatment did not alter the area or volume of angiotensin II treated VSMCs (**Figure 7A-C**) or VSMCs incubated in growth media for 18 hours (**Figure 7E-G**) on pliable hydrogels, compared to their vehicle control treated counterparts. In contrast, TCAQP1 treatment reduced the area and volume of both angiotensin II stimulated VSMCs (**Figure 7A-C**) and VSMCs incubated in growth media for 18 hours (**Figure 7E-G**) on rigid hydrogels, compared to their vehicle treated counterparts. No changes in VSMC height were observed in any condition (**Figure 7D and H**).

To elucidate signalling components regulating aquaporin-1, we next screened inhibitors of known components of volume regulation in other cell types. VSMC area was unaltered by pretreatment with a concentration response of the NKCC blocker, furosemide and the WNK inhibitor, STOCK2S 26016, prior to angiotensin II stimulation on rigid hydrogels (**Supplementary Figure S13**). However, VSMC area was reduced by pretreatment with a concentration response of the PKC inhibitor Go 6983, prior to angiotensin II stimulation on rigid hydrogels (**Supplementary Figure S14**). Confocal microscopy confirmed that Go 6983 treatment did not alter the area or volume of VSMCs incubated in growth media for 18 hours (**Figure 8A-C**) on pliable hydrogels, compared to their vehicle control treated counterparts. In contrast, Go 6983 treatment reduced the area and volume of VSMCs incubated in growth media for 18 hours (**Figure 8A-C**) on rigid hydrogels, compared to their vehicle treated counterparts. No changes in VSMC height were observed in any condition (**Figure 8D**).

PKC positively regulates aquaporin-1 activity in *Xenopus* oocytes and promotes aquaporin-1 membrane translocation in HEK cells (Conner et al., 2010). Therefore, we next determined aquaporin-1 localisation in VSMCs on pliable and rigid hydrogels. Analysed revealed that aquaporin-1 was distributed in both the nucleus and cytoplasm of angiotensin II stimulated VSMCs on 12 and 72 kPa hydrogels (**Supplementary Figure S15A**). Closer examination revealed that aquaporin-1 localised more towards the basal membrane in angiotensin II stimulated VSMCs on pliable hydrogels (**Supplementary Figure S15A and B**). In contrast, aquaporin-1 was redistributed towards that apical membrane of angiotensin II stimulated VSMCs on rigid hydrogels (**Supplementary Figure S15A and B**). We next determined the impact of PKC inhibition on aquaporin-1 localisation. Analysis revealed that Go 6983 pretreatment prior to angiotensin II treatment resulted in a redistribution of aquaporin-1 to the nucleus in VSMCs on pliable (**Supplementary Figure S15C and D**) and rigid (**Figure 8E and F**) hydrogels.

3.6 Piezo1 and aquaporin-1 expression are upregulated in disease relevant modified VSMC phenotypes

We next assessed the relevance of this mechanism in disease. Recent studies have demonstrated substantial heterogeneity of VSMCs in both human disease and murine experimental models, including atherosclerosis and vascular injury (Dobnikar et al., 2018; Wirka et al., 2019; Pan et al., 2020). We therefore examined the gene expression of piezo1 and aquaporin-1 (Aqp1) across VSMC-derived cell types in vivo using available scRNA-seq dataset from lineage traced VSMCs in vascular disease models. After acute injury, Aqp1 and Piezo1 mRNA levels were higher in VSMC-derived cells that have reduced contractile gene expression, but express Tnfrsf11, Vcam1 and Ly6a (**Figure 9 and Supplementary Figure S16**).

Tnfrsf11 is a marker of modulated VSMCs in human and mouse atherosclerosis (Wirka et al., 2019) and Ly6a, that encodes stem cell antigen 1 (SCA1), is a marker of activated VSMCs that are predisposed to proliferate (Worssam et al., 2023). Both genes were also expressed in proliferating Mki67+ cells (**Figure 9, Supplementary Figure S16A**). In contrast, the paralogues Aqp2, Aqp3 and Piezo2 showed little expression across the population (**Supplementary Figure S16**). Hierarchical clustering analysis confirmed that the expression pattern of Piezo1 and Aqp1 is similar to that of genes characteristic of VSMC activation markers (Ly6a/Vcam1/Tnfrsf11b) across a trajectory connecting Myh11-high and proliferating cells (**Figure 9B**). In VSMC-derived cells isolated from high-fat diet induced atherosclerotic lesions in Apoe-/- animals, Aqp1 expression was elevated in Ly6a+ cells (**Supplementary Figure S16**). Piezo1 levels was generally lower but also detected more frequently in cells with low Myh11 levels (**Supplementary Figure S16**). This analysis is consistent with increased functional importance of aquaporin-1 and piezo1 in VSMCs in disease compared to contractile cells in healthy arteries.

4. Discussion

Our understanding of how changes in the mechanical environment of the aortic wall drives VSMC dysfunction and the VSMC derived mechanisms that contribute to the decreased aortic compliance observed in ageing and CV disease remains limited. Previous studies have shown that ECM rigidity promotes VSMC dedifferentiation, a process where VSMCs downregulate contractile markers whilst increasing the expression of proliferative genes (Brown et al., 2010; Sazonova et al., 2015; Nagayama and Nishimiya, 2020). Increased ECM rigidity has also been reported to stimulate VSMC migration, adhesion and proliferation (Wong et al., 2003; Brown et al., 2010; Sazonova et al., 2015; Nagayama and Nishimiya, 2020; Rickel et al., 2020). Furthermore, in response to matrix rigidity, VSMC reorganise their actin cytoskeleton and generate enhanced traction stresses (Brown et al., 2010; Sazonova et al., 2015; Petit et al., 2019; Sanyour et al., 2019). We now show that contractile agonist stimulation of quiescent VSMCs on pliable (healthy) or rigid (aged/diseased) matrices results in a differential response; VSMCs on pliable matrices decreased in area as they contracted, whereas increased cell area was observed in VSMCs on rigid matrices. Furthermore, on rigid matrices, contractile agonist stimulation also promoted an increase in VSMC volume. These findings suggest that changes in VSMC morphology following contractile agonist stimulation are differentially regulated on pliable and rigid matrices. On pliable matrices, actomyosin activity promotes contraction and VSMC area subsequently decreases but volume remains unchanged. In contrast, on rigid matrices, changes in VSMC morphology are driven by enhanced volume. We identify for the first time that enhanced matrix rigidity initiates an increased volume response within VSMCs.

Hypertension is regarded as one of the strongest risk factors for the progression of CV disease (Kjeldsen, 2018). VSMCs dedifferentiate as a result of hypertension, becoming dysfunctional and hypertrophic (Touyz et al., 2018). VSMC hypertrophy is comprised of both an increase in volume and an increase in protein synthesis. Our findings suggest that increased VSMC volume is an early event that persists in response to enhanced matrix rigidity. Importantly, VSMC hypertrophy contributes to aortic wall thickening, increased aortic

stiffness and reduced aortic compliance, which in turn leads to hypertension (Brown et al., 2018). The causality between VSMC hypertrophy and hypertension is cyclic in nature, with the development of one promoting the onset of the other. Current methods of investigating VSMC hypertrophy generally utilise animal models, including rat models of hypertension and genetic depletion in mice (Owens and Schwartz, 1983; Hixon et al., 2000; Choi et al., 2019; Bai et al., 2021). We now show that the *in vitro* induction of increased VSMC volume can be achieved through culturing cells on rigid matrices. This enables the mechanisms regulating VSMC volume control to be investigated at a greater throughput.

In hypertension, VSMC Ca^{2+} handling is known to become dysregulated, with VSMCs entering a hypercontractile state that further increases aortic rigidity whilst simultaneously reducing aortic compliance (Touyz et al., 2018). Our findings suggest that the internal release of Ca^{2+} from the sarcoplasmic reticulum, following angiotensin II stimulation, is required for both contraction and the increased volume response stimulated by increased ECM rigidity. In addition to the release of Ca^{2+} from internal stores, the increased VSMC volume response is driven by the extracellular influx of Ca^{2+} through mechanosensitive SACs. Specifically, we identify piezo1 as a driver of ECM rigidity induced VSMC swelling. VSMC piezo1 expression is upregulated in mouse models of atherosclerosis and abdominal aortic aneurysms, with dysregulation of VSMC mechanosensation shown to drive these disease states (Qian et al., 2022; Yin et al., 2022). Our findings show that on pliable hydrogels, Ca^{2+} flux is tightly regulated, and angiotensin II treatment triggered a rapid Ca^{2+} intracellular spike that rapidly dissipated. In contrast, angiotensin II treatment of rigid hydrogels triggered a prolonged/sustained increase in intracellular Ca^{2+}. This sustained Ca^{2+} signal was blocked by GsMTx-4 treatment and was recapitulated by using the piezo1 specific allosteric activator Yoda1. Interestingly, piezo1 activity appeared to be only partially activated by actomyosin activity on rigid hydrogels and multiple Ca^{2+} peaks were observed that evidentially resulted in a sustained activation. Potentially, actomyosin activity contributed to transient activation of piezo1 and eventually triggers sustained activation of a subset of piezo1 channels. Piezo1 has been shown to localise in close proximity to integrin-mediated cell matrix adhesions and an intriguing possibility is that adhesion associated tension contributes to piezo1 activation (Yao et al., 2022). Another possibility is that piezo1 possess delayed off-kinetics on rigid hydrogels. Potentially, piezo1 channels open on both pliable and rigid matrices following angiotensin stimulation, but the off kinetics of piezo1 are highly rapid on pliable matrices. Piezo1 opening at physiological rigidities exhibits rapid on- and off-kinetics and matrix rigidity driven changes in the off kinetics may explain this pathophysiological mechanism. Yoda1 treatment resulted in full activation of piezo1 in angiotensin II treated VSMCs on pliable and rigid hydrogels, which resulted in increased VSMC volume on pliable hydrogels. This finding confirms that piezo1 mediated Ca^{2+} influx initiates increased VSMC volume. However, VSMC volume failed to increase further in Yoda1 treated VSMCs on rigid hydrogels, suggesting that the rigidity induced VSMC pathway is already at maximum capacity in rigid environments. More research is needed to better understand the subsets and the localisation/associations of piezo1 that contribute to this response.

Downstream of piezo1, we identify PKC and aquaporin-1 as key components of this VSMC response to enhanced ECM rigidity. VSMCs are known to express aquaporin-1, but the

functional significance of aquaporin-1 in VSMCs has remained elusive (Shanahan et al., 1999). Our findings suggest that piezo1–mediated Ca^{2+} influx activates PKC, which in turn promotes increased membrane translocation of aquaporin-1, driving increased VSMC volume. Importantly, our analysis of single cell sequencing datasets revealed that both piezo1 and aquaporin-1 are upregulated in phenotypically modified VSMC populations. This suggests that VSMC phenotypic modulation observed in vascular diseases, including atherosclerosis and abdominal aortic aneurysms, results in increased piezo1 and aquaporin-1 levels in VSMCs. Furthermore, increased aortic wall rigidity is observed in both atherosclerosis and abdominal aortic aneurysms (Glasser et al., 1997; Mitchell et al., 2010; Lacolley et al., 2017), suggesting that the phenotypically modified VSMCs potentially activate this ECM rigidity induced pathway to increase VSMC volume under conditions of increased aortic wall stiffness observed in hypertension and other aortic diseases. Increased VSMC volume will potentially further reduce the compliance of the aortic wall due to increased VSMC-derived hydrostatic forces being placed on the aortic wall. Increased VSMC volume will also reduce the compressibility of the aortic wall and will potentially further alter the biomechanical landscape of the aortic wall. Further research to test these findings in *ex vivo* and *in vivo* settings are essential next steps in confirming the validity of our findings and to better understand how matrix rigidity induced changes in VSMC volume contribute to the biomechanical properties of the aortic wall.

Whilst our findings have generated new mechanistic insight into a previously unknown VSMC response to matrix rigidity, our study does have a number of limitations. Firstly, we use a single cell, two-dimensional approach. Although this allows the interrogation of signalling pathways linked to VSMC function, it is different to VSMC organisation in the aortic wall. In vivo, these aortic VSMCs are in a three-dimensional environment and are in contact with other VSMCs via cell-cell adhesions. The VSMCs used in this study are primary human aortic VSMCs and this accounts for the variability in our data. We cannot rule out the possibility that cell-cell contacts and ECM topology also contribute to VSMC matrix rigidity responses. Piezo1 activity has also been reported to be driven by surface roughness, so a better understanding of ECM topology, curvature and roughness is now needed to understand the precise triggers for this VSMC volume response (Bavi et al., 2019). Despite these limitations, our findings highlight the power of our approach in unravelling previously unknown mechanisms that potentially participate in disease/age associated VSMC dysfunction. These findings now require validation in *ex vivo* and *in vivo* systems in order to further support the validity of our approach, but the potential importance of our findings are further highlighted by gene expression profiles of single cell sequencing datasets that showed increased piezo1 and aquaporin-1 gene expression in disease relevant VSMC phenotypes. Taken together, we identify a novel pathway that drives increased VSMC volume in rigid environments. Our findings also suggest that key components of this volume control pathway are upregulated in VSMC phenotypes that are prevalent in aortic disease.

Author Contributions: RTJ, RS, FW, SA, JCKT, JR, GA, JM, HFJ and DTW were responsible for performing experiments and analysing data. DTW analysed data. CJM, HFJ, SB and DTW were

involved in the conceptualisation of the study. CJM and SB reviewed and edited this manuscript. DTW and HFJ were responsible for the design, writing and editing of this manuscript. RTJ assisted with the writing the initial version of the manuscript.

Acknowledgements: This work was funded by a Biotechnology and Biological Sciences Research Council Research Grant (BB/T007699/1) and a British Heart Foundation PhD Studentship (FS/17/32/32916) awarded to DTW and a UKRI Biotechnology and Biological Sciences Research Council Norwich Research Park Doctoral Training Partnership PhD Studentship awarded to FW (BB/T008717/1).

Conflict of Interests: The authors declare that the research was conducted in the absence of any commercial or financial relationships that could be construed as a potential conflict of interest.

Data Availability: The data that support the findings of this study are available from the corresponding author upon reasonable request.

Declaration of transparency and scientific rigour: This Declaration acknowledges that this paper adheres to the principles for transparent reporting and scientific rigour of preclinical research as stated in the BJP guidelines for Natural Products Research, Design and Analysis, and Immunoblotting and Immunochemistry, and as recommended by funding agencies, publishers and other organisations engaged with supporting research.

References

Ahmed, S., Johnson, Robert.T., Solanki, R., Afewerki, T., Wostear, F., and Warren, Derek.T. (2022). Using Polyacrylamide Hydrogels to Model Physiological Aortic Stiffness Reveals that Microtubules Are Critical Regulators of Isolated Smooth Muscle Cell Morphology and Contractility. Frontiers in Pharmacology *13*: 836710.

Ahmed, S., and Warren, D.T. (2018). Vascular smooth muscle cell contractile function and mechanotransduction. Vessel Plus *2*: 36.

Alexander, S.P.H., Christopoulos, A., Davenport, A.P., Kelly, E., Mathie, A., Peters, J.A., et al. (2021). THE CONCISE GUIDE TO PHARMACOLOGY 2021/22: G protein-coupled receptors. British J Pharmacology *178*:.

Bai, L., Kee, H.J., Choi, S.Y., Seok, Y.M., Kim, G.R., Kee, S.-J., et al. (2021). HDAC5 inhibition reduces angiotensin II-induced vascular contraction, hypertrophy, and oxidative stress in a mouse model. Biomedicine & Pharmacotherapy *134*: 111162.

Bavi, N., Richardson, J., Heu, C., Martinac, B., and Poole, K. (2019). PIEZO1-Mediated Currents Are Modulated by Substrate Mechanics. ACS Nano *13*: 13545–13559.

Brown, I.A.M., Diederich, L., Good, M.E., DeLalio, L.J., Murphy, S.A., Cortese-Krott, M.M., et al. (2018). Vascular Smooth Muscle Remodeling in Conductive and Resistance Arteries in Hypertension. Arteriosclerosis, Thrombosis, and Vascular Biology *38*: 1969–1985.

Brown, X.Q., Bartolak-Suki, E., Williams, C., Walker, M.L., Weaver, V.M., and Wong, J.Y. (2010). Effect of substrate stiffness and PDGF on the behavior of vascular smooth muscle cells: implications for atherosclerosis. J Cell Physiol *225*: 115–122.

Choi, S.Y., Kee, H.J., Sun, S., Seok, Y.M., Ryu, Y., Kim, G.R., et al. (2019). Histone deacetylase inhibitor LMK235 attenuates vascular constriction and aortic remodelling in hypertension. Journal of Cellular and Molecular Medicine *23*: 2801–2812.

Conner, M.T., Conner, A.C., Brown, J.E.P., and Bill, R.M. (2010). Membrane Trafficking of Aquaporin 1 Is Mediated by Protein Kinase C via Microtubules and Regulated by Tonicity. Biochemistry *49*: 821–823.

Curtis, M.J., Alexander, S., Cirino, G., Docherty, J.R., George, C.H., Giembycz, M.A., et al. (2018). Experimental design and analysis and their reporting II: updated and simplified guidance for authors and peer reviewers. British Journal of Pharmacology *175*: 987–993.

Dobnikar, L., Taylor, A.L., Chappell, J., Oldach, P., Harman, J.L., Oerton, E., et al. (2018). Disease-relevant transcriptional signatures identified in individual smooth muscle cells from healthy mouse vessels. Nat Commun *9*: 4567.

Eggermont, J., Trouet, D., Carton, I., and Nilius, B. (2001). Cellular function and control of volume-regulated anion channels. Cell Biochem Biophys *35*: 263–274.

Emig, R., Knodt, W., Krussig, M.J., Zgierski-Johnston, C.M., Gorka, O., Groß, O., et al. (2021). Piezo1 Channels Contribute to the Regulation of Human Atrial Fibroblast Mechanical Properties and Matrix Stiffness Sensing. Cells *10*: 663.

Glasser, S.P., Arnett, D.K., McVeigh, G.E., Finkelstein, S.M., Bank, A.J., Morgan, D.J., et al. (1997). Vascular Compliance and Cardiovascular Disease: A Risk Factor or a Marker? American Journal of Hypertension *10*: 1175–1189.

Hayashi, K., and Naiki, T. (2009). Adaptation and remodeling of vascular wall; biomechanical response to hypertension. Journal of the Mechanical Behavior of Biomedical Materials *2*: 3–19.

Hayenga, H.N., Trache, A., Trzeciakowski, J., and Humphrey, J.D. (2011). Regional atherosclerotic plaque properties in ApoE-/- mice quantified by atomic force, immunofluorescence, and light microscopy. J Vasc Res *48*: 495–504.

Hixon, M.L., Muro-Cacho, C., Wagner, M.W., Obejero-Paz, C., Millie, E., Fujio, Y., et al. (2000). Akt1/PKB upregulation leads to vascular smooth muscle cell hypertrophy and polyploidization. J Clin Invest *106*: 1011–1020.

Hoffmann, E.K., Lambert, I.H., and Pedersen, S.F. (2009). Physiology of Cell Volume Regulation in Vertebrates. Physiological Reviews *89*: 193–277.

Johnson, R.T., Solanki, R., and Warren, D.T. (2021). Mechanical programming of arterial smooth muscle cells in health and ageing. Biophys Rev *13*: 757–768.

Kjeldsen, S.E. (2018). Hypertension and cardiovascular risk: General aspects. Pharmacological Research *129*: 95–99.

Kobayashi, T., and Sokabe, M. (2010). Sensing substrate rigidity by mechanosensitive ion channels with stress fibers and focal adhesions. Current Opinion in Cell Biology *22*: 669–676.

Lacolley, P., Regnault, V., and Laurent, S. (2020). Mechanisms of Arterial Stiffening. Arteriosclerosis, Thrombosis, and Vascular Biology *40*: 1055–1062.

Lacolley, P., Regnault, V., Segers, P., and Laurent, S. (2017). Vascular Smooth Muscle Cells and Arterial Stiffening: Relevance in Development, Aging, and Disease. Physiological Reviews *97*: 1555–1617.

Leloup, A.J.A., Van Hove, C.E., De Moudt, S., De Meyer, G.R.Y., De Keulenaer, G.W., and Fransen, P. (2019). Vascular smooth muscle cell contraction and relaxation in the isolated aorta: a critical regulator of large artery compliance. Physiological Reports *7*: e13934.

Li, M., Zhang, X., Wang, M., Wang, Y., Qian, J., Xing, X., et al. (2022). Activation of Piezo1 contributes to matrix stiffness-induced angiogenesis in hepatocellular carcinoma. Cancer Communications *42*: 1162–1184.

Liu, S., and Lin, Z. (2022). Vascular Smooth Muscle Cells Mechanosensitive Regulators and Vascular Remodeling. JVR *59*: 90–113.

Lopez-Cavestany, M., Hahn, S.B., Hope, J.M., Reckhorn, N.T., Greenlee, J.D., Schwager, S.C., et al. (2023). Matrix stiffness induces epithelial-to-mesenchymal transition via Piezo1-regulated calcium flux in prostate cancer cells. iScience *26*: 106275.

Lowis, C., Winaya, A., Kumari, P., Rivera, C., Vlahos, J., Hermantara, R., et al. (2023). Mechanosignals in abdominal aortic aneurysms. Frontiers in Cardiovascular Medicine *9*: 1021934.

McManus, M.L., Churchwell, K.B., and Strange, K. (1995). Regulation of Cell Volume in Health and Disease. New England Journal of Medicine *333*: 1260–1267.

Minaisah, R.-M., Cox, S., and Warren, D.T. (2016). The Use of Polyacrylamide Hydrogels to Study the Effects of Matrix Stiffness on Nuclear Envelope Properties. In The Nuclear Envelope, S. Shackleton, P. Collas, and E.C. Schirmer, eds. (New York, NY: Springer New York), pp 233–239.

Mitchell, G.F., Hwang, S.-J., Vasan, R.S., Larson, M.G., Pencina, M.J., Hamburg, N.M., et al. (2010). Arterial Stiffness and Cardiovascular Events. Circulation *121*: 505–511.

Mola, M.G., Sparaneo, A., Gargano, C.D., Spray, D.C., Svelto, M., Frigeri, A., et al. (2016). The speed of swelling kinetics modulates cell volume regulation and calcium signaling in astrocytes: A different point of view on the role of aquaporins. Glia *64*: 139–154.

Morishita, K., Watanabe, K., and Ichijo, H. (2019). Cell volume regulation in cancer cell migration driven by osmotic water flow. Cancer Science *110*: 2337–2347.

Nagayama, K., and Nishimiya, K. (2020). Moderate substrate stiffness induces vascular smooth muscle cell differentiation through cellular morphological and tensional changes. Biomed Mater Eng *31*: 157–167.

Nourse, J.L., and Pathak, M.M. (2017). How cells channel their stress: Interplay between Piezo1 and the cytoskeleton. Seminars in Cell & Developmental Biology *71*: 3–12.

Owens, G.K., and Schwartz, S.M. (1983). Vascular smooth muscle cell hypertrophy and hyperploidy in the Goldblatt hypertensive rat. Circulation Research *53*: 491–501.

Pan, H., Xue, C., Auerbach, B.J., Fan, J., Bashore, A.C., Cui, J., et al. (2020). Single-Cell Genomics Reveals a Novel Cell State During Smooth Muscle Cell Phenotypic Switching and Potential Therapeutic Targets for Atherosclerosis in Mouse and Human. Circulation *142*: 2060–2075.

Petit, C., Guignandon, A., and Avril, S. (2019). Traction Force Measurements of Human Aortic Smooth Muscle Cells Reveal a Motor-Clutch Behavior. Molecular and Cellular Biomechanics.

Porter, L., Minaisah, R.-M., Ahmed, S., Ali, S., Norton, R., Zhang, Q., et al. (2020). SUN1/2 Are Essential for RhoA/ROCK-Regulated Actomyosin Activity in Isolated Vascular Smooth Muscle Cells. Cells *9*: 132.

Qian, W., Hadi, T., Silvestro, M., Ma, X., Rivera, C.F., Bajpai, A., et al. (2022). Microskeletal stiffness promotes aortic aneurysm by sustaining pathological vascular smooth muscle cell mechanosensation via Piezo1. Nat Commun *13*: 512.

Qiu, H., Zhu, Y., Sun, Z., Trzeciakowski, J.P., Gansner, M., Depre, C., et al. (2010). Short Communication: Vascular Smooth Muscle Cell Stiffness As a Mechanism for Increased Aortic Stiffness With Aging. Circulation Research *107*: 615–619.

Ragnauth, C.D., Warren, D.T., Liu, Y., McNair, R., Tajsic, T., Figg, N., et al. (2010). Prelamin A Acts to Accelerate Smooth Muscle Cell Senescence and Is a Novel Biomarker of Human Vascular Aging. Circulation *121*: 2200–2210.

Rezvani-Sharif, A., Tafazzoli-Shadpour, M., and Avolio, A. (2019). Progressive changes of elastic moduli of arterial wall and atherosclerotic plaque components during plaque development in human coronary arteries. Med Biol Eng Comput *57*: 731–740.

Rickel, A.P., Sanyour, H.J., Leyda, N.A., and Hong, Z. (2020). Extracellular Matrix Proteins and Substrate Stiffness Synergistically Regulate Vascular Smooth Muscle Cell Migration and Cortical Cytoskeleton Organization. ACS Appl. Bio Mater. *3*: 2360–2369.

Rizzoni, D., Porteri, E., Guefi, D., Piccoli, A., Castellano, M., Pasini, G., et al. (2000). Cellular Hypertrophy in Subcutaneous Small Arteries of Patients With Renovascular Hypertension. Hypertension *35*: 931–935.

Safar, M.E., Henry, O., and Meaume, S. (2002). Aortic Pulse Wave Velocity: An Independent Marker of Cardiovascular Risk. The American Journal of Geriatric Cardiology *11*: 295–304.

Sanyour, H.J., Li, N., Rickel, A.P., Childs, J.D., Kinser, C.N., and Hong, Z. (2019). Membrane cholesterol and substrate stiffness co-ordinate to induce the remodelling of the cytoskeleton and the alteration in the biomechanics of vascular smooth muscle cells. Cardiovasc Res *115*: 1369–1380.

Sazonova, O.V., Isenberg, B.C., Herrmann, J., Lee, K.L., Purwada, A., Valentine, A.D., et al. (2015). Extracellular matrix presentation modulates vascular smooth muscle cell mechanotransduction. Matrix Biology *41*: 36–43.

Sazonova, O.V., Lee, K.L., Isenberg, B.C., Rich, C.B., Nugent, M.A., and Wong, J.Y. (2011). Cell-Cell Interactions Mediate the Response of Vascular Smooth Muscle Cells to Substrate Stiffness. Biophysical Journal *101*: 622–630.

Schiffrin, E.L. (2012). Vascular Remodeling in Hypertension. Hypertension *59*: 367–374.

Schindelin, J., Arganda-Carreras, I., Frise, E., Kaynig, V., Longair, M., Pietzsch, T., et al. (2012). Fiji: an open-source platform for biological-image analysis. Nat Methods *9*: 676–682.

Sehgel, N.L., Sun, Z., Hong, Z., Hunter, W.C., Hill, M.A., Vatner, D.E., et al. (2015a). Augmented Vascular Smooth Muscle Cell Stiffness and Adhesion When Hypertension Is Superimposed on Aging. Hypertension *65*: 370–377.

Sehgel, N.L., Vatner, S.F., and Meininger, G.A. (2015b). "Smooth Muscle Cell Stiffness Syndrome"—Revisiting the Structural Basis of Arterial Stiffness. Frontiers in Physiology *6*:.

Sehgel, N.L., Zhu, Y., Sun, Z., Trzeciakowski, J.P., Hong, Z., Hunter, W.C., et al. (2013). Increased vascular smooth muscle cell stiffness: a novel mechanism for aortic stiffness in hypertension. American Journal of Physiology-Heart and Circulatory Physiology *305*: H1281–H1287.

Sequí-Domínguez, I., Cavero-Redondo, I., Álvarez-Bueno, C., Pozuelo-Carrascosa, D.P., Nuñez de Arenas-Arroyo, S., and Martínez-Vizcaíno, V. (2020). Accuracy of Pulse Wave Velocity Predicting Cardiovascular and All-Cause Mortality. A Systematic Review and Meta-Analysis. Journal of Clinical Medicine *9*: 2080.

Shanahan, C.M., Connolly, D.L., Tyson, K.L., Cary, N.R.B., Osbourn, J.K., Agre, P., et al. (1999). Aquaporin-1 Is Expressed by Vascular Smooth Muscle Cells and Mediates Rapid Water Transport across Vascular Cell Membranes. JVR *36*: 353–362.

Touyz, R.M., Alves-Lopes, R., Rios, F.J., Camargo, L.L., Anagnostopoulou, A., Arner, A., et al. (2018). Vascular smooth muscle contraction in hypertension. Cardiovascular Research *114*: 529–539.

Tracqui, P., Broisat, A., Toczek, J., Mesnier, N., Ohayon, J., and Riou, L. (2011). Mapping elasticity moduli of atherosclerotic plaque in situ via atomic force microscopy. J Struct Biol *174*: 115–123.

Tsamis, A., Krawiec, J.T., and Vorp, D.A. (2013). Elastin and collagen fibre microstructure of the human aorta in ageing and disease: a review. Journal of The Royal Society Interface *10*: 20121004.

Warren, D.T., Tajsic, T., Porter, L.J., Minaisah, R.M., Cobb, A., Jacob, A., et al. (2015). Nesprin-2-dependent ERK1/2 compartmentalisation regulates the DNA damage response in vascular smooth muscle cell ageing. Cell Death Differ *22*: 1540–1550.

Wirka, R.C., Wagh, D., Paik, D.T., Pjanic, M., Nguyen, T., Miller, C.L., et al. (2019). Atheroprotective roles of smooth muscle cell phenotypic modulation and the TCF21 disease gene as revealed by single-cell analysis. Nat Med *25*: 1280–1289.

Wong, J.Y., Velasco, A., Rajagopalan, P., and Pham, Q. (2003). Directed Movement of Vascular Smooth Muscle Cells on Gradient-Compliant Hydrogels. Langmuir *19*: 1908–1913.

Woodrum, D.A., and Brophy, C.M. (2001). The paradox of smooth muscle physiology. Molecular and Cellular Endocrinology *177*: 135–143.

Worssam, M.D., Lambert, J., Oc, S., Taylor, J.C.K., Taylor, A.L., Dobnikar, L., et al. (2023). Cellular mechanisms of oligoclonal vascular smooth muscle cell expansion in cardiovascular disease. Cardiovasc Res *119*: 1279–1294.

Wu, Y., Xu, X., Liu, F., Jing, Z., Shen, D., He, P., et al. (2023). Three-Dimensional Matrix Stiffness Activates the Piezo1-AMPK-Autophagy Axis to Regulate the Cellular Osteogenic Differentiation. ACS Biomater. Sci. Eng. *9*: 4735–4746.

Yao, M., Tijore, A., Cheng, D., Li, J.V., Hariharan, A., Martinac, B., et al. (2022). Force- and cell state–dependent recruitment of Piezo1 drives focal adhesion dynamics and calcium entry. Sci. Adv. *8*: eabo1461.

Yin, Q., Zang, G., Li, N., Sun, C., and Du, R. (2022). Agonist-induced Piezo1 activation promote mitochondrial-dependent apoptosis in vascular smooth muscle cells. BMC Cardiovasc Disord *22*: 287.

Zhang, Y., Griendling, K.K., Dikalova, A., Owens, G.K., and Taylor, W.R. (2005). Vascular Hypertrophy in Angiotensin II–Induced Hypertension Is Mediated by Vascular Smooth Muscle Cell–Derived H2O2. Hypertension *46*: 732–737.

Zhong, Q., Hu, M.-J., Cui, Y.-J., Liang, L., Zhou, M.-M., Yang, Y.-W., et al. (2018). Carotid–Femoral Pulse Wave Velocity in the Prediction of Cardiovascular Events and Mortality: An Updated Systematic Review and Meta-Analysis. Angiology *69*: 617–629.

Zieman, S.J., Melenovsky, V., and Kass, D.A. (2005). Mechanisms, Pathophysiology, and Therapy of Arterial Stiffness. Arteriosclerosis, Thrombosis, and Vascular Biology *25*: 932–943.

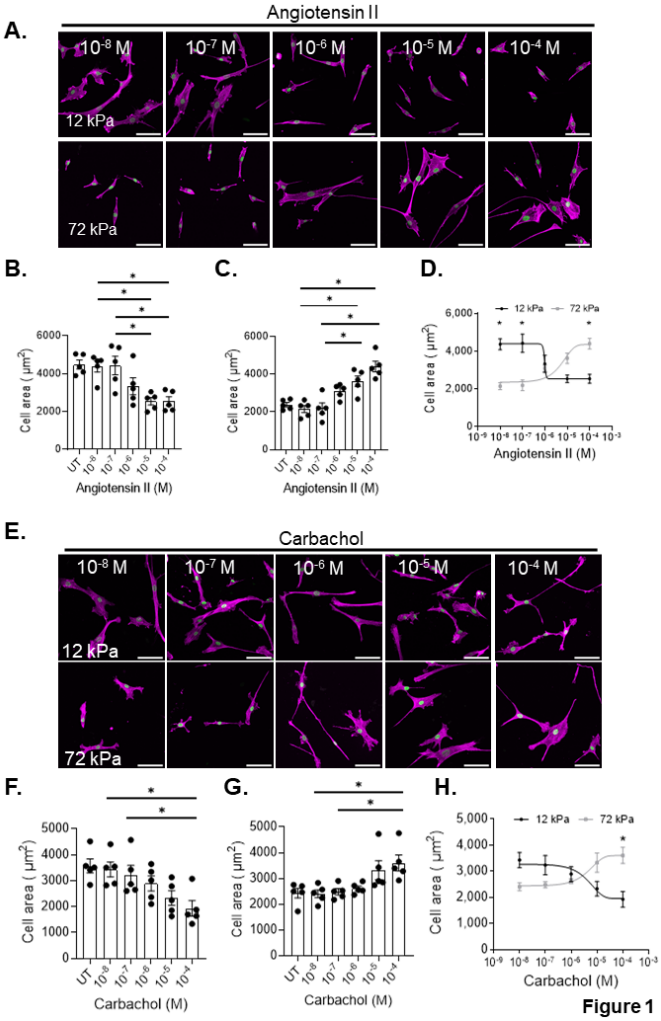

Figure 1

Figure 1. VSMC response to contractile agonist stimulation is matrix stiffness dependent. Representative images of isolated VSMCs cultured on 12 or 72 kPa polyacrylamide hydrogels. Actin cytoskeleton (purple) and Lamin A/C labelled nuclei (green). Scale bar = 100 µm. A) VSMCs were treated with increasing concentrations of angiotensin II (0.01 – 100 µM) for 30 minutes. VSMC area on (B) 12 kPa and (C) 72 kPa hydrogels. Graphs show the means of each individual repeat (black dots) of 5 independent experiments with ≥158 cells analysed per condition. Significance determined using a one-way ANOVA followed by Tukey's test. (D) Comparison of VSMC response to angiotensin II on 12 and 72 kPa hydrogels. Data is expressed as the mean of individual repeats calculated from 5 independent experiments; significance determined using a two-way ANOVA followed by Sidak's test. (E) VSMCs were treated with increasing concentrations of carbachol (0.01 – 100 µM) for 30 minutes. VSMC area on (F) 12 kPa and (G) 72 kPa hydrogels representative of 5 independent experiments with ≥149 cells analysed per condition. Significance determined using a one-way ANOVA followed by Tukey's test. (H) Comparison of VSMC response to carbachol on 12 and 72 kPa hydrogels. Data is expressed as the mean of the means calculated from 5 independent experiments, mean data of each individual repeat is shown as a black dot; significance determined using a two-way ANOVA followed by Turkey's multiple comparison test. (* = $p < 0.05$, error bars represent ± SEM).

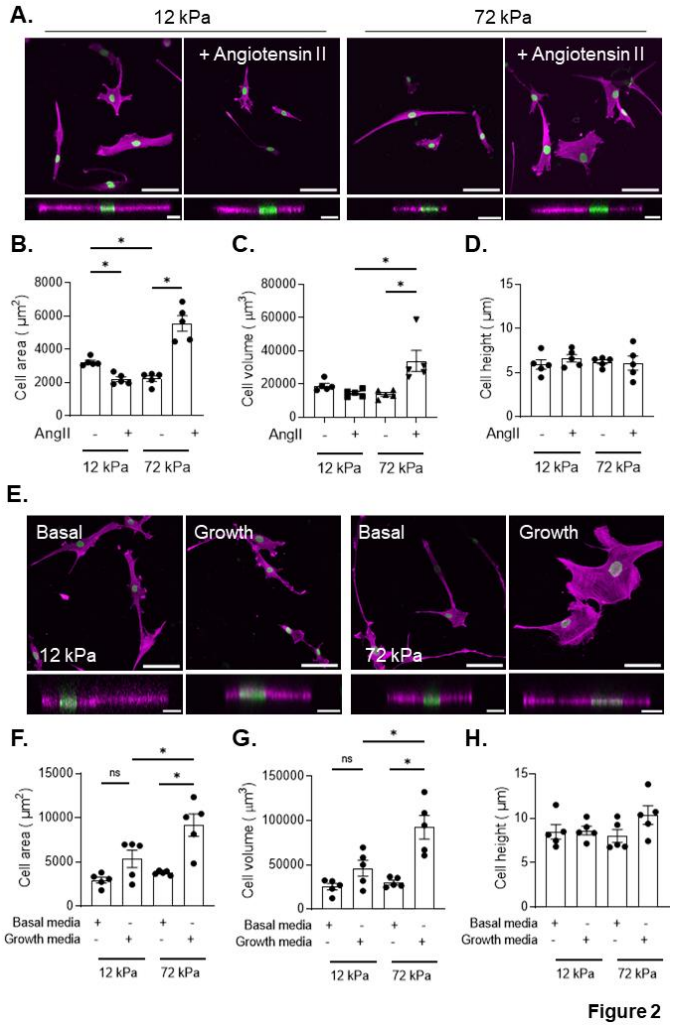

Figure 2

Figure 2. VSMC display increased volume on rigid substrates. A) Representative images of isolated VSMCs cultured on 12 or 72 kPa polyacrylamide hydrogels treated with angiotensin II (AngII) (10 µM). Actin cytoskeleton (purple) and DAPI labelled nuclei (green). Top – Representative XY images of VSMC area, scale bar = 100 µm. Bottom – Representative XZ images of VSMC height, scale bar = 20 µm. Graphs show B) VSMC area, C) VSMC volume and D) VSMC height and represent the combined data from 5 independent experiments with ≥82 cells analysed per condition. Mean data from each individual repeat of the 5 independent experiments is shown by a black dot. Significance was determined using two-way ANOVA followed by Tukey's test. E) Representative images of isolated VSMCs seeded on 12 or 72 kPa polyacrylamide hydrogels incubated in basal or growth media for 24 hours. Actin cytoskeleton (purple) and DAPI labelled nuclei (green). Top panel shows representative XY images of VSMC area, scale bar = 100 µm. Bottom panel shows representative XZ images of VSMC height, scale bar = 20 µm. Graphs show VSMC F) area, G) volume and H) height and represent the combined data from 5 independent experiments with ≥50 cells analysed per condition. Mean data from each individual repeat of the 5 independent experiments is shown by a black dot. Significance was determined using two-way ANOVA followed by Tukey's multiple comparison test.

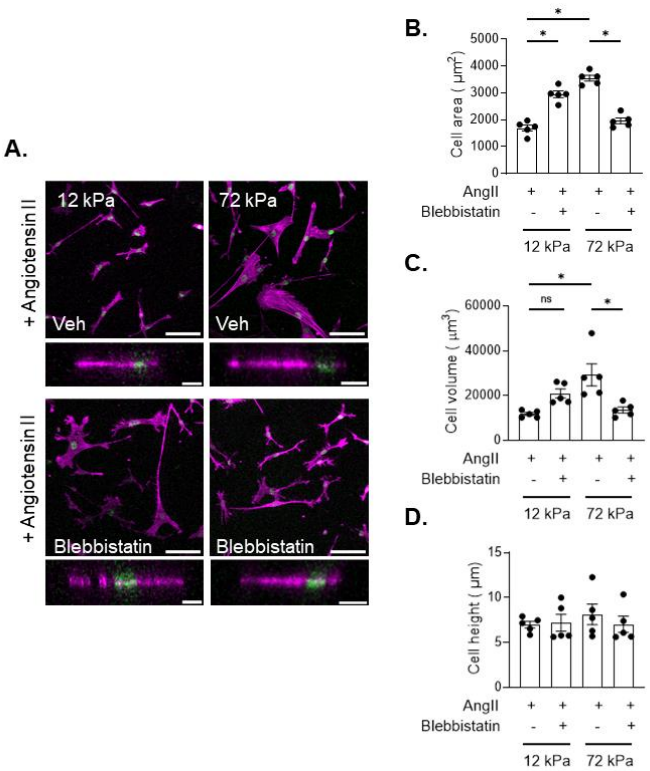

Figure 3

Figure 3. Intracellular tension is required for the increased VSMC volume observed following angiotensin II stimulation of VSMCs on rigid hydrogels. A) Representative images of vehicle control (DMSO) and blebbistatin treated angiotensin II stimulated VSMCs on 12 and 72 kPa hydrogels. Actin cytoskeleton (purple) and DAPI labelled nuclei (green). Top panel shows representative XY images of VSMC area, scale bar = 100 μm. Bottom panel shows representative XZ images of VSMC height, scale bar = 20 μm. Graphs show VSMC B) area, C) volume and D) height and represent the combined data from 5 independent experiments with ≥60 cells analysed per condition. Mean data from each individual repeat of the 5 independent experiments is shown by a black dot. Significance was determined using two-way ANOVA followed by Tukey's multiple comparison test.

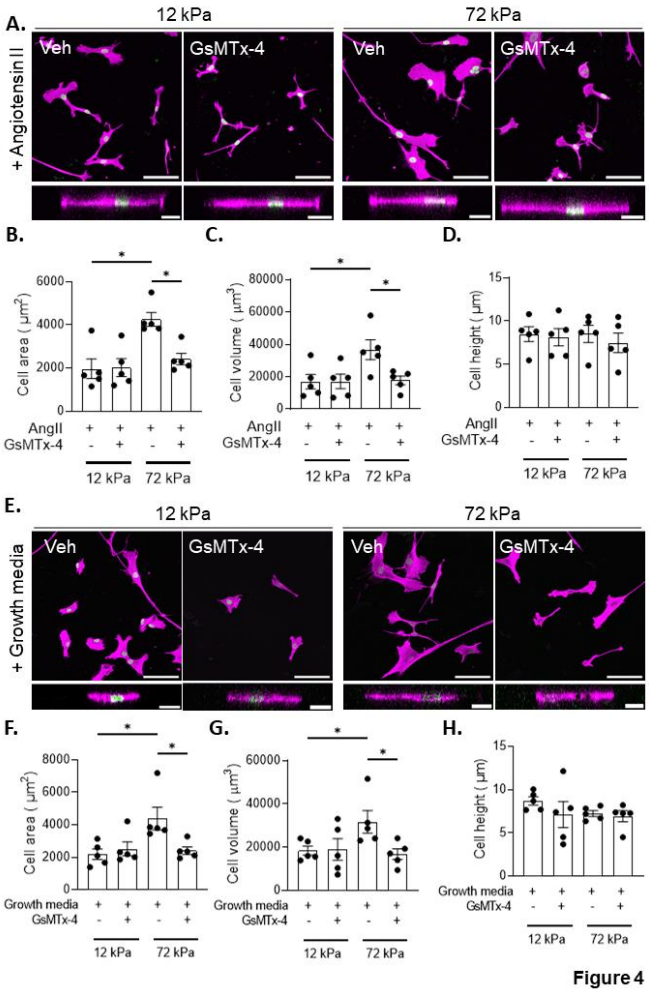

Figure 4

Figure 4. SAC blockade reduces VSMC volume on rigid hydrogels. A) Representative images of isolated VSMCs cultured on 12 or 72 kPa polyacrylamide hydrogels treated with angiotensin II (AngII) (10 µM) in the presence of vehicle control (dH_2O) or GsMTx-4. Actin cytoskeleton (purple) and DAPI labelled nuclei (green). Top panel shows representative XY images of VSMC area, scale bar = 100 µm. Bottom panel shows representative XZ images of VSMC height, scale bar = 20 µm. Graphs show VSMC B) area, C) volume and D) height and represent the combined data from 5 independent experiments with ≥74 cells analysed per condition. Mean data from each individual repeat of the 5 independent experiments is shown by a black dot. Significance was determined using two-way ANOVA followed by Tukey's test. E) Representative images of isolated VSMCs seeded on 12 or 72 kPa polyacrylamide hydrogels incubated in basal or growth media for 18 hours in the presence of vehicle control (dH_20) or GsMTx-4. Actin cytoskeleton (purple) and DAPI labelled nuclei (green). Top panel shows representative XY images of VSMC area, scale bar = 100 µm. Bottom panel shows representative XZ images of VSMC height, scale bar = 20 µm. Graphs show VSMC F) area, G) volume and H) height and represent the combined data from 5 independent experiments with ≥50 cells analysed per condition. Mean data from each individual repeat of the 5 independent experiments is shown by a black dot. Significance was determined using two-way ANOVA followed by Turkey's multiple comparison test.

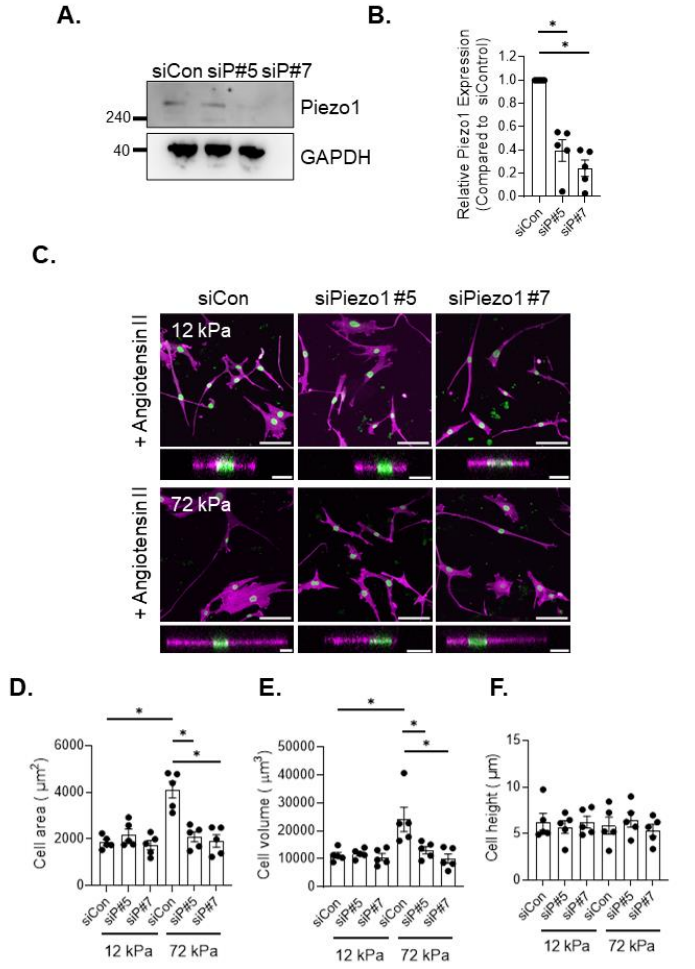

Figure 5

Figure 5. Piezo1 depletion reduces VSMC volume on rigid hydrogels. A) Representative Western blot and (B) densitometric analysis of siRNA mediated piezo1 depletion. Data representative of 5 independent experiments, individual values for the 5 independent experiments are shown as a black dot in B). Significance determined using a one-way ANOVA followed by Dunnett's test. C) Representative images of scrambled siRNA control (siCon) or piezo1-depleted VSMCs cultured on 12 or 72 kPa hydrogels following angiotensin II (10 µM) stimulation. Actin cytoskeleton (purple) and lamin A/C labelled nuclei (green). Top panel shows representative XY images of VSMC area, scale bar = 100 µm. Bottom panel shows representative XZ images of VSMC height, scale bar = 20 µm. Graphs show VSMC D) area, E) volume and F) height and represent the combined data of 5 independent experiments with ≥60 cells analysed per condition. Mean data for each individual repeat of the 5 independent experiments is shown as a black dot. Significance determined using a two-way ANOVA followed by Tukey's multiple comparison test. (* = $p < 0.05$, error bars represent ± SEM).

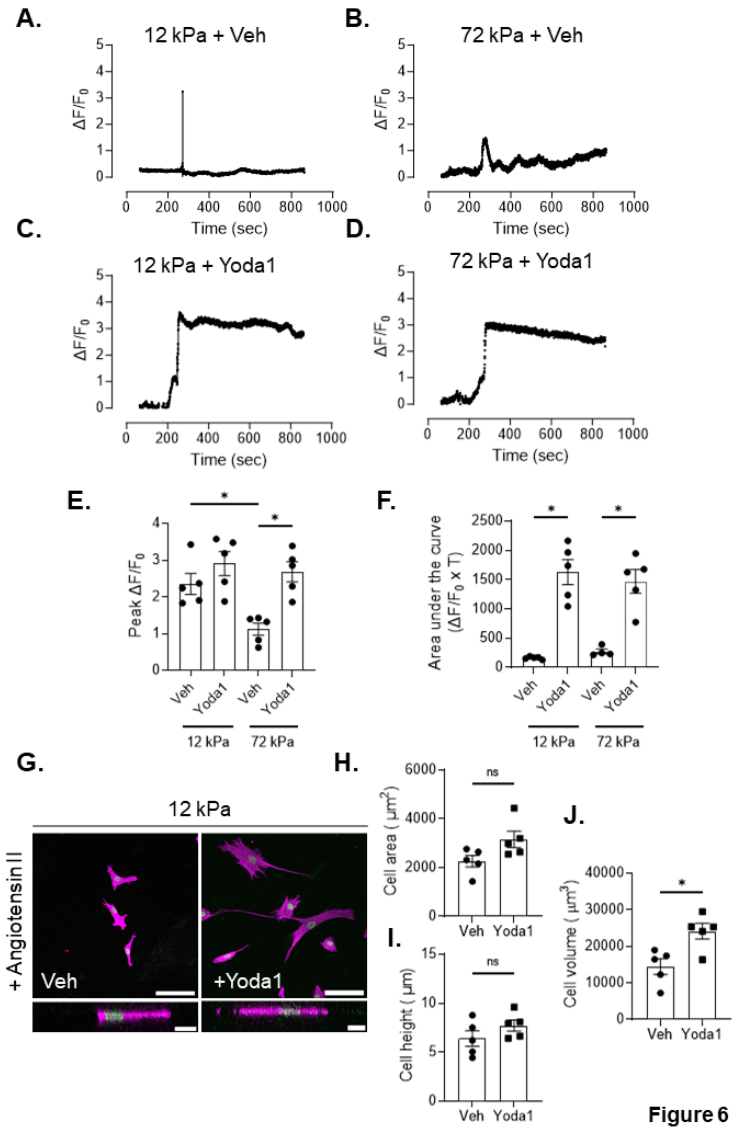

Figure 6. Extracellular calcium influx via piezo1 ion channels triggers increased VSMC volume on pliable hydrogels. Quiescent VSMCs were Fluo-4 loaded on 12 and 72 kPa hydrogels. Graphs show representative $\Delta F/F_0$ values over time for A) vehicle and C) Yoda1 treated angiotensin II stimulated VMSCs on 12 kPa hydrogels; and B) vehicle and D) Yoda1 treated angiotensin II stimulated VSMCs on 72 kPa hydrogels. Each graph represents the mean data of 6 individual cells and is representative of a single experiment. Graphs show E) peak $\Delta F/F_0$ value and F) area under the curve values. Mean data for individual repeats of the 5 independent experiments are shown as black dots. Significance was determined using two-way ANOVA followed by Tukey's multiple comparison test. G) Representative images of vehicle control (DMSO) and Yoda1 treated angiotensin II stimulated VSMCs on 12 kPa hydrogels. Actin cytoskeleton (purple) and DAPI labelled nuclei (green). Top panel shows representative XY images of VSMC area, scale bar = 100 μm. Bottom panel shows representative XZ images of VSMC height, scale bar = 20 μm. Graphs show VSMC H) area, I) volume and J) height and represent the combined data from 5 independent experiments with ≥54 cells analysed per condition. Mean data from each individual repeat of the 5 independent experiments is shown by a black dot. Significance was determined using unpaired student t-test.

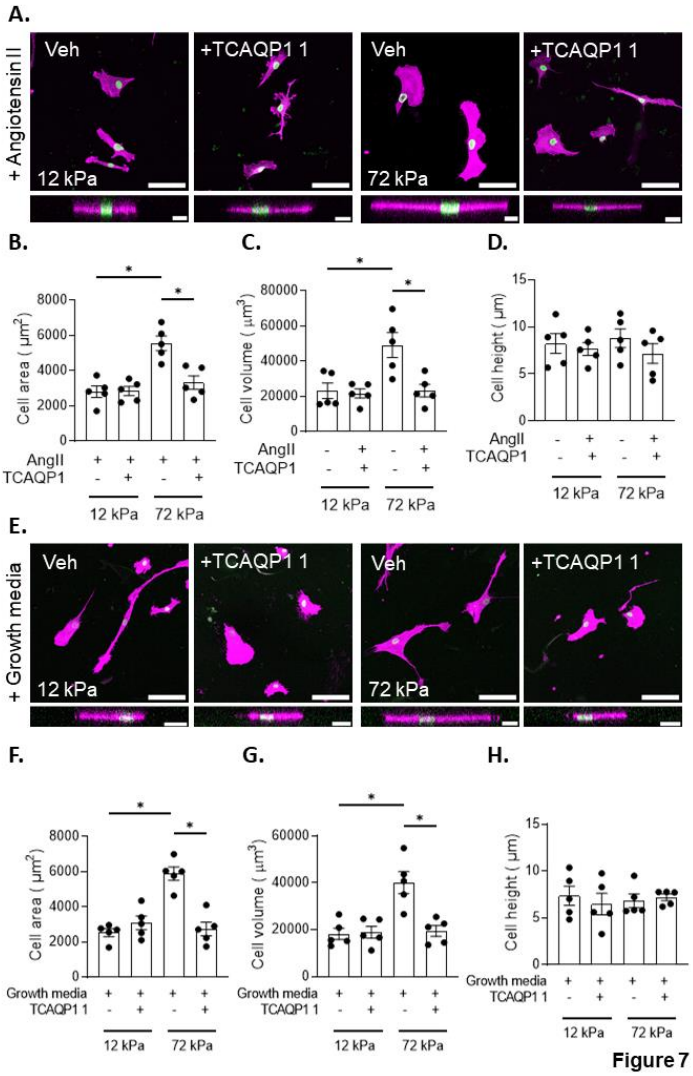

Figure 7

Figure 7. Aquaporin-1 inhibition reduces VSMC volume on rigid hydrogels. A) Representative images of isolated VSMCs cultured on 12 or 72 kPa polyacrylamide hydrogels treated with angiotensin II (AngII) (10 µM) in the presence of vehicle control (DMSO) or TCAQP1. Actin cytoskeleton (purple) and DAPI labelled nuclei (green). Top panel shows representative XY images of VSMC area, scale bar = 100 µm. Bottom panel shows representative XZ images of VSMC height, scale bar = 20 µm. Graphs show B) VSMC area, C) VSMC volume and D) VSMC height and represent the combined data from 5 independent experiments with ≥62 cells analysed per condition. Mean data from individual repeats of the 5 independent experiments is shown by a black dot. Significance was determined using two-way ANOVA followed by Tukey's multiple comparison test. E) Representative images of isolated VSMCs seeded on 12 or 72 kPa polyacrylamide hydrogels incubated in basal or growth media for 18 hours in the presence of vehicle control (DMSO) or TCAQP1. Actin cytoskeleton (purple) and DAPI labelled nuclei (green). Top panel shows representative XY images of VSMC area, scale bar = 100 µm. Bottom panel shows representative XZ images of VSMC height, scale bar = 20 µm. Graphs show F) VSMC area, G) VSMC volume and H) VSMC height and represent the combined data from 5 independent experiments with ≥55 cells analysed per condition. Mean data from each individual repeat of the 5 independent experiments is shown by a black dot. Significance was determined using two-way ANOVA followed by Tukey's multiple comparison test.

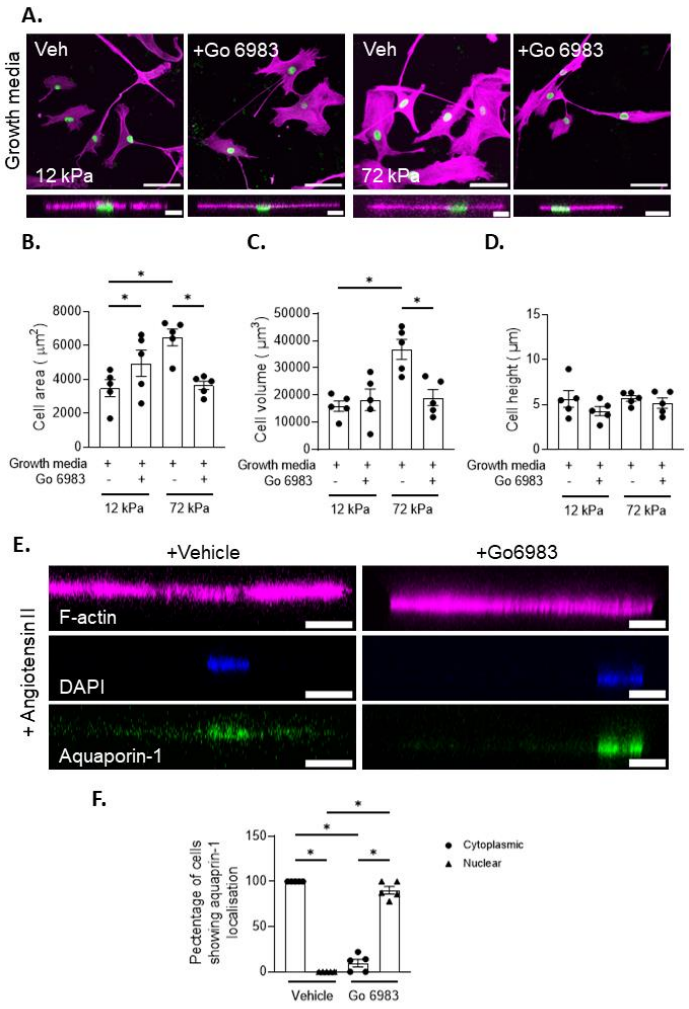

Figure 8

Figure 8. PKC inhibition reduces VSMC volume on rigid hydrogels. A) Representative images of isolated VSMCs seeded on 12 or 72 kPa polyacrylamide hydrogels incubated in basal or growth media for 18 hours in the presence of vehicle control (DMSO) or Go 6983. Actin cytoskeleton (purple) and DAPI labelled nuclei (green). Top panel shows representative XY images of VSMC area, scale bar = 100 µm. Bottom panel shows representative XZ images of VSMC height, scale bar = 20 µm. Graphs show F) VSMC area, G) VSMC volume and H) VSMC height and represent the combined data from 5 independent experiments with ≥45 cells analysed per condition. Mean data from each individual repeat of the 5 independent experiments is shown by a black dot. Significance was determined using two-way ANOVA followed by Tukey's multiple comparison test. E) Representative XZ images of aquaporin-1 (green), DAPI (blue) and F-actin (purple) organisation in angiotensin II stimulated VSMCs on 72 kPa hydrogels treated with either vehicle control (DMSO) or Go 6983 prior to angiotensin II stimulation. Scale bar = 20 µm. F) Graph shows percentage of VSMCs displaying cytoplasmic and nuclear localisation of aquaporin-1 and represents the combined data of 5 independent experiments with ≥42 cells analysed per condition. Mean data of individual repeats of the 5 independent experiments are shown as black dots (cytoplasmic) or black triangles (nuclear). Significance determined using a one-way ANOVA followed by Tukey's multiple comparison test. (* = $p < 0.05$, error bars represent ± SEM).

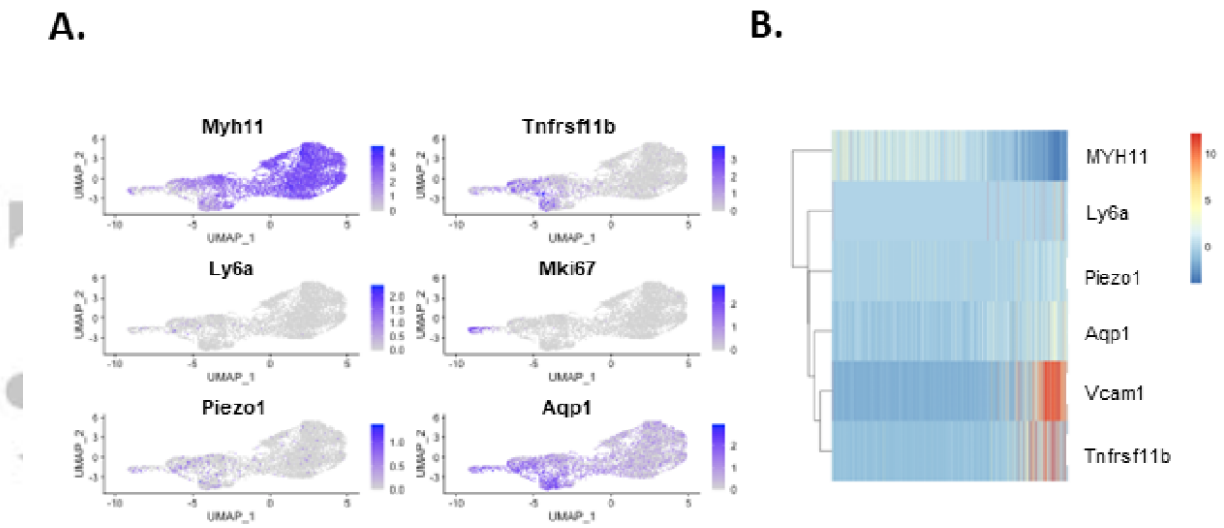

Figure 9. Piezo1 and aquaporin-1 are upregulated in disease-relevant phenotypically modified VSMCs. Analysis of scRNA-seq data from VSMC-derived cells isolated 5 days after vascular injury (Worssam et al., 2023). (A) Projections showing expression of markers *Piezo1* and *Aqp1* across the cell populations. For reference, the expression of markers for the contractile state (*Myh11*), modulated/synthetic VSMCs (*Tnfrsf11b*), activated VSMCs in a transition state (*Ly6a*), and cell proliferation (*Mki67*) are also provided. (B) Heat map showing scaled expression values for *Aqp1*, *Piezo1*, markers of activated VSMCs (*Vcam1*, *Ly6a*), the synthetic VSMC marker *Tnfrsf11b*, contractile gene *Myh11* in VSMCs ordered according to progression along an inferred trajectory that connects Myh11^{-high} and proliferating cells.

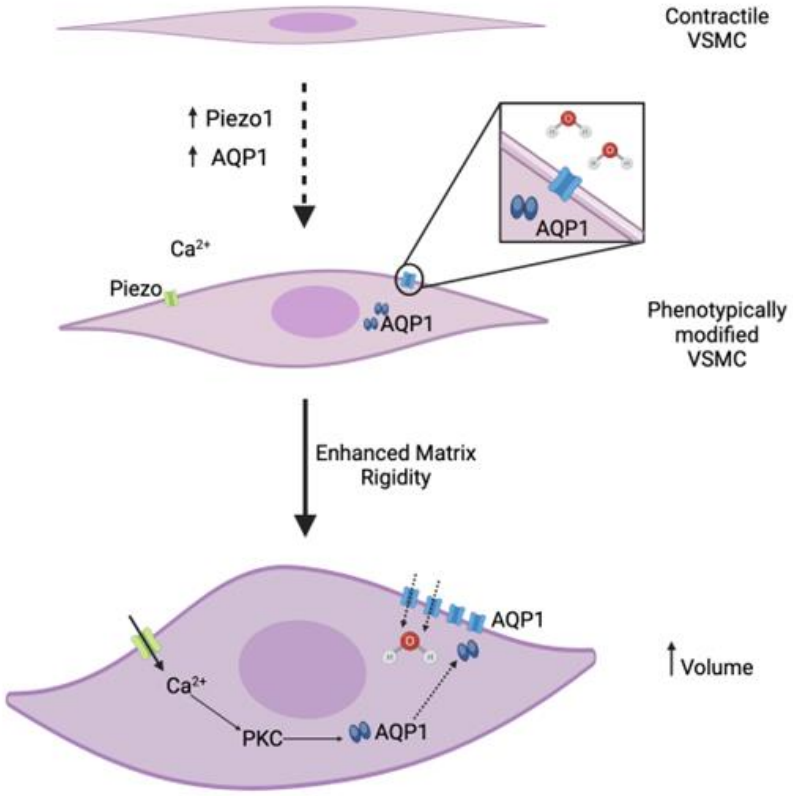

Graphical Abstract